LED Pulser System for Fermilab's DØ Muon Scintillation Counters

P.Hanlet[1,5], S.Doulas[1], N.Kirsch[1], M.Marcus[1,6], D.Wood[1]
H.Haggerty[2], S.Hansen[2], A.S.Ito[2], R.Jones[2], T.Regan[2]
B.S.Acharya[3], S.Dugad[3], B.Satyanarayana[3]
J.Pablo Negret[4], M.Zanabria[4]

1. Northeastern University, Boston, MA 02115
2. Fermi National Accelerator Laboratory, Batavia, IL 60510
3. Tata Institute of Fundamental Research, Colaba, Mumbai 40005, India
4. Universidad de los Andes, Bogota, Columbia
5. presently at Illinios Institute of Technology, Chicago, IL 60616
6. presently at University of Wisconsin, Madison, WI 53706

Abstract

We present the technical design, performance, and stability test results for an LED based pulser system. The system is used for the Run II Muon Scintillation counters at Fermilab's DØ Experiment. Accurate timing information from the scintillation counters is imperative for the proper performance of the muon triggers. The LED Pulser System served in the commissioning of the counters and continues to serve in the monitoring of the performance and the gains of the PMTs.

A detailed description of the system is presented, as well as the results of tests on individual components and integrated system. From the test results, the DØ LED Pulser System tracks the PMT gains with a precision of 0.2%.

1 Introduction

We present a design for the LED Pulser System for the Fermilab, DØ muon scintillation counters. The purpose of this pulser system is to provide means for testing, commissioning, calibrating, and monitoring the gains and timings of the counters. The system described is based on a modified version of the system that was successfully used by the E760 collaboration for monitoring their electromagnetic calorimeter photomultiplier tubes, or *PMTs*[1].

The DØ Run II muon system, described in detail in other documents[2], con-

Preprint submitted to Elsevier Science *2 December 2002*

tains three sets of scintillation counters. The central pseudo-rapidity [1] region, covers the range ($|\eta| \lesssim 1$); it consists of up to three radial layers of scintillation counters referred to as *CMSC—Central Muon Scintillation Counters*[3]. The forward regions cover ($1 \lesssim |\eta| \lesssim 2$) and have six—3 north and 3 south—planes of counters, or *FMSC—Forward Muon Scintillation Counters*[4], in an η–ϕ pixel geometry with respect to the beam axis. Both types of counters are scintillator sheets with wavelength shifting fibers or bars embedded to carry the light to the PMTs. The CMSC uses BCF-91A or BCF-92 wavelength shifting fiber and Thorn EMI 9902KA PMTs; the FMSC uses Kumarin 40 wavelength shifting bars and Melz 115 PMTs.

The muon scintillator system is used to tag, or *trigger* on, real muons that are temporally coincident with events of interest. Scintillation counters have a fast response time, as compared to wire chambers, so they can be used to trigger muon candidates at the first trigger level. This implies the correct timing of muon signals is imperative to the operation of the muon trigger. This can be seen in Fig. 1, which shows the time spectrum for hits in muon scintillation test counters placed during Run I in the nearest radial layer of the DØ muon system at $\eta = 0$ and $\eta = 1.1$. In the figure, the bold distribution shows the muon spectrum for the counter at $\eta = 0$; here one sees a large background of out–of–time muons with a clear (shaded) peak of in–time muons.

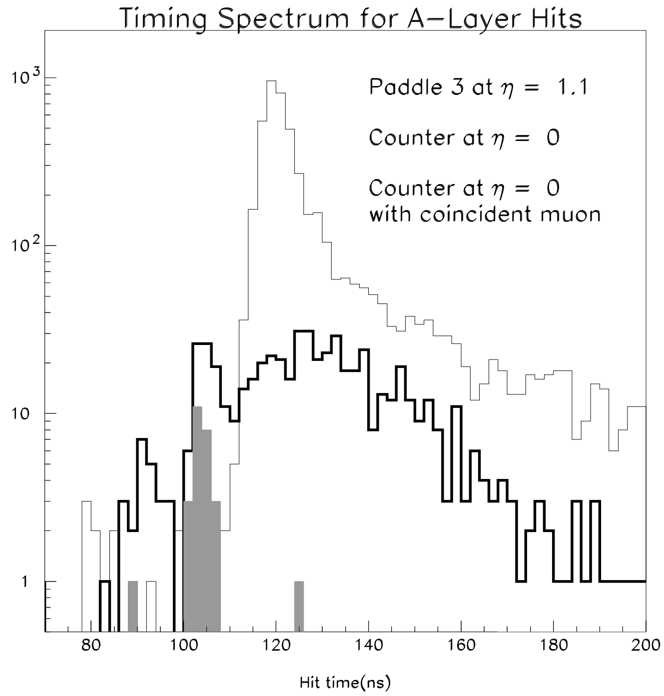

Fig. 1. Run I Muon Scintillator Time Spectrum: bold distribution is for counter at η=0

[1] pseudo-rapidity, or η, is related to the tangential angle θ with respect to a beam axis, $\eta = -ln(tan(\frac{\theta}{2}))$.

1.1 *Motivation for an LED Pulser System*

Our experience during Run IB with the 240 counters[3] has guided us to design and install a calibration system with an external light source. An LED pulser system allows us to: (1) trivially find dead PMTs, (2) isolate the behavior of the PMTs from the front end electronics, (3) monitor PMT gains, (4) track timing changes with threshold and voltage changes, and (5) perform controlled burn in of the PMTs.

Fig. 2 shows an example of how a change in the PMT gain—shown as ΔV—translates to a signal timing change Δt. For example, for a 10 ns risetime a 10% gain change corresponds to a $\Delta t = 1$ ns signal timing shift. The LED Pulser System serves to continuously monitor PMT gains so as to flag counters which fall out of tolerance. Since all PMT signals have a risetime of < 10 ns, monitoring of the gains to a 10% level will insure proper timing of all counters for the muon trigger. With the system described in this report, we have exceeded this requirement.

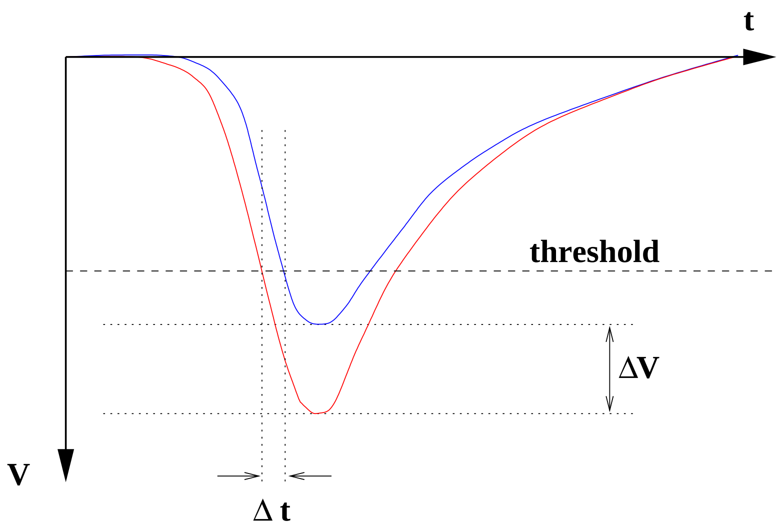

Fig. 2. Example of how the trigger timing changes with PMT gain change

1.2 *Specifications*

The following are the requirements for an external light calibration system: (1) a short duration light pulse with <10 ns rise time, (2) a fall time of ~ 30 or ~ 50 ns, (3) a variable amplitude signal in the MIP range, (4) a variable delay capability, (5) a 200Hz rate capability, (6) a capability to distribute light pulses to each scintillation counter, (7) a control capability directed by the DØ controls system, (8) a match of emission spectra of LEDs and wavelength shifting fibers(bars) in the central(forward) regions, and (9) system stability against temperature or voltage fluctuations, noisy environment, and magnetic fields.

In what follows, we present the details of a system which meets the above specifications. We start by describing the major components of the LED Pulser System. This is followed by test results of uniformity and stability, system control, results using the system, and conclusions.

2 System Design

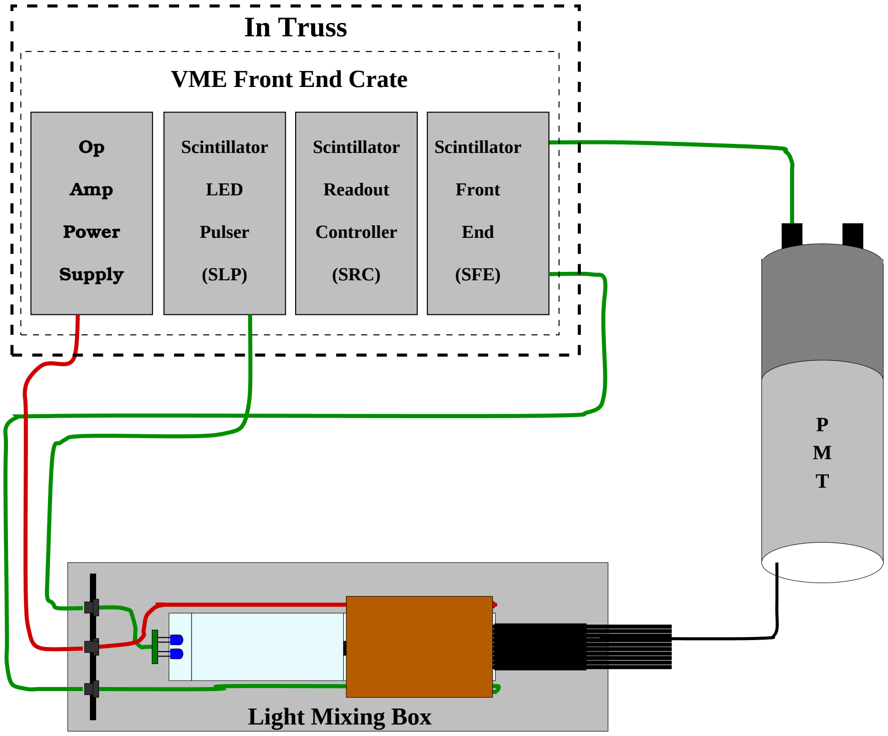

Fig. 3. Diagram of LED Pulser System for single channel (not to scale)

The LED Pulser System is an integral part of the DØ Online and Data Acquisition systems, with all of the necessary control, monitoring, and analysis capabilities.

The LED Pulser System consists of seven major components: [2] (1) Scintillator LED Pulser, *(SLP)*, (2) LED Driver Board, *(LDB)*, (3) LED Block, (4) Light Mixing Blocks, (5) Light Distribution and Strain Relief *(Fiber Block)*, (6) System Monitoring via *PIN Photodiode/Amplifier*, and (7) Readout.

[2] The reader is referred to [5,6] for detailed descriptions of the muon readout system.

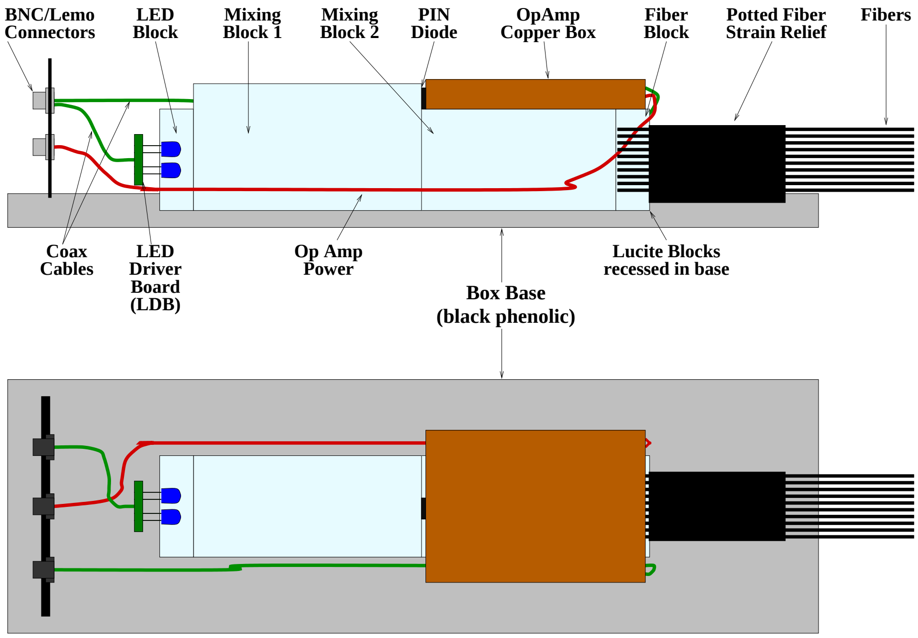

Fig. 4. Light Mixing Box Components

An example of the scintillator calibration and monitoring system for one channel is shown in Fig. 3. In the figure, the VME based Scintillator LED Pulser, or *SLP*, generates a pulse to trigger the LED Driver Board, or *LDB*, which drives the LEDs potted in the LED block. The light is then mixed in two lucite mixing blocks and is distributed to individual PMTs via fiber optic cables. The mixed light to the PMTs is monitored using a PIN Photodiode, or *PIN* Diode, which is located downstream of the first mixing block; this signal is amplified using an OpAmp circuit and line driver. The LDB, LED Block, Mixing Blocks, and Fiber Block are all housed in the Light Mixing Box, or *LMB*, as shown in Fig. 4. Both the PMT and OpAmp signals are read out using standard Scintillator Front End, *SFE*, readout cards[6].

2.1 The Scintillator LED Pulser

The Scintillator LED Pulser[5,6], *SLP*, is a custom designed $9U\times280$ mm VME board. There is one SLP in each VME front end crate for scintillators. A block diagram of the SLP is shown in Fig. 5. The Scintillator Readout Controller, or *SRC*, is in the same front end crate and communicates with the SLP via the VME backplane.

The SLP performs the following functions: (1) accepts VME back plane trigger, (2) accepts an LVDS—Low Voltage Digital Signal—test pulse trigger from the SRC via the backplane, (3) accepts NIM external test pulse from front panel lemo connector, (4) accepts front panel push button trigger, (5) allows VME controlled individual channel enable, (6) allows VME controlled individual channel amplitude adjustment, (7) allows VME controlled individual channel delay adjustment, (8) outputs each of 12 channel's LED driver signal via front panel lemo connectors, and (9) illuminates front panel display LED when channel is output.

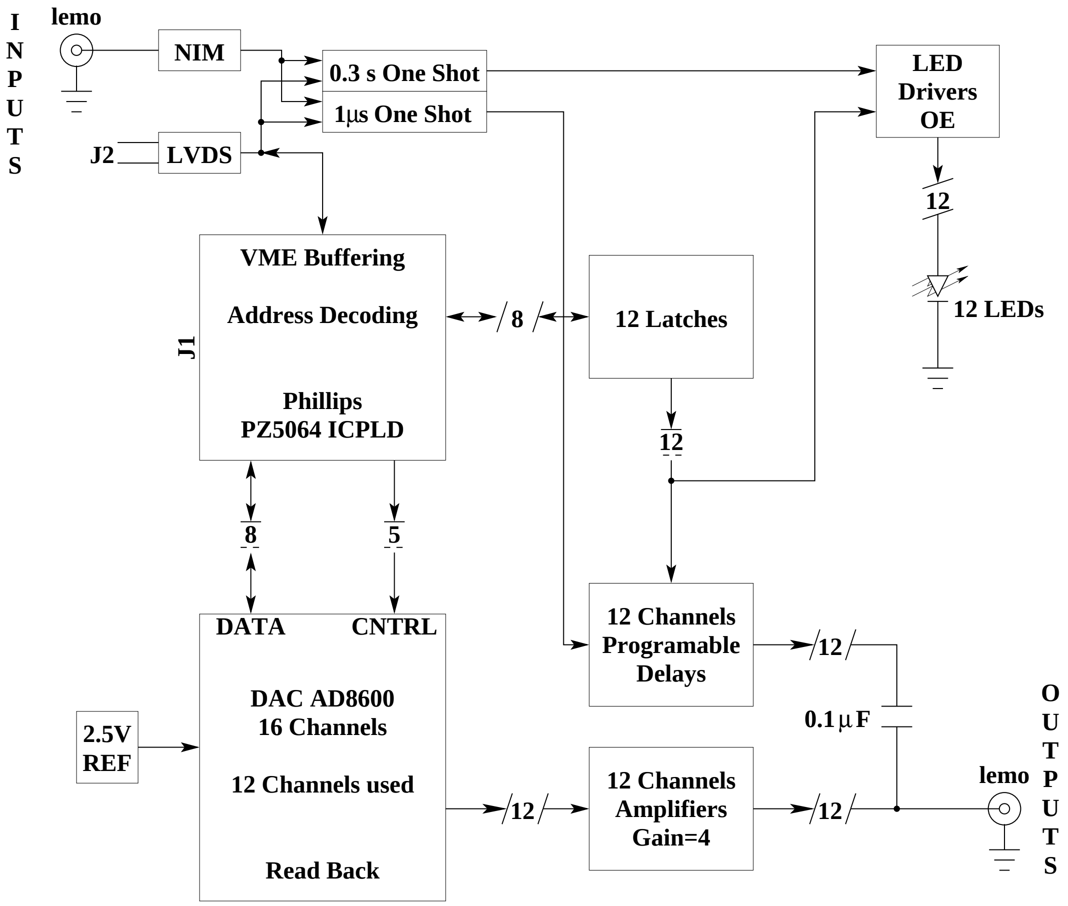

Fig. 5. Block Diagram of the SLP

The SLP outputs 12 channels of a DC offset TTL signal; each channel is enabled by a VME controlled 12–bit R/W channel enable register. The DC offset for each channel is set by the VME controlled 8–bit R/W DAC and is limited to a 2.5 V maximum output. The DAC output is then amplified by a $4\times$ OpAmp, yielding a 10 V maximum output, and added resistively to the TTL signal. The variable delay of each channel is set by a VME controlled R/W register which controls two programmable delay lines of 8 20ns steps and 16 2ns steps. Each channel is designed to have an amplitude stability of $<1\%$ and a channel–to–channel time slew of <1 ns.

The LED Driver Board, Fig. 6, delivers a negative going differentiated pulse to each of the four LEDs in an LED block. The circuit operates by charging and subsequently discharging a capacitor when a TTL trigger pulse is received from the SLP module. The pulse amplitude is determined by the DC offset of the SLP output. This allows both timing and amplification of the pulse to be controlled over a single coaxial cable from the SLP. The leading edge rise time is designed to be <8 ns. The trailing edge fall time is controlled by values of RC and is selected to have a $\sim 50(30)$ ns time constant in the CMSC(FMSC). This pulse shape was designed to best match a MIP signal from muons in FMSC and CMSC counters while still using only one LDB design. For the blue LEDs, Sec. 2.3, the capacitor value was chosen to be 330 pF; for the bluish-green LEDs, the capacitor value is 390 pF.

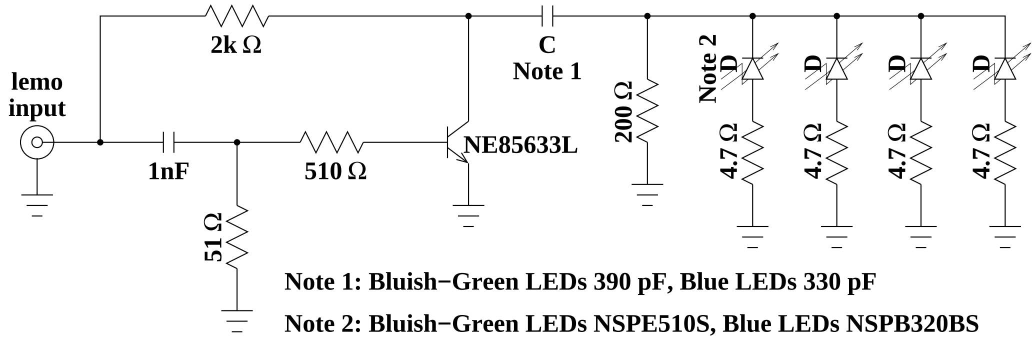

Fig. 6. LED Driver Board: LDB

The LDB is located inside the LMB and is soldered directly to the LEDs in the LED block. The input signal is transported from the SLP to the LMB via RG58-U coaxial cable. Within the box, the SLP signal is fed through a BNC/lemo bulkhead connector on the front face of the LMB, and on to the LDB via RG174-U coaxial cable.

In order to ensure that the manufacturer specified current limit for the LEDs is not violated, a current limiting resistor is placed on each LED leg of the circuit. The current limiting resistor value of $R = 4.7\Omega$ was chosen such that at the maximum SLP output of 10 V, each LED has a maximum current of <100 mA.

2.3 LED Block

An LED block is a lucite block with four LEDs potted in the block. The dimensions and LED positions are shown in Fig. 7. Since the drilling procedure for the LED holes sometimes caused crazing in the lucite, the blocks were annealed at 230°F for 3 hours to insure that the blocks would not crack in time.

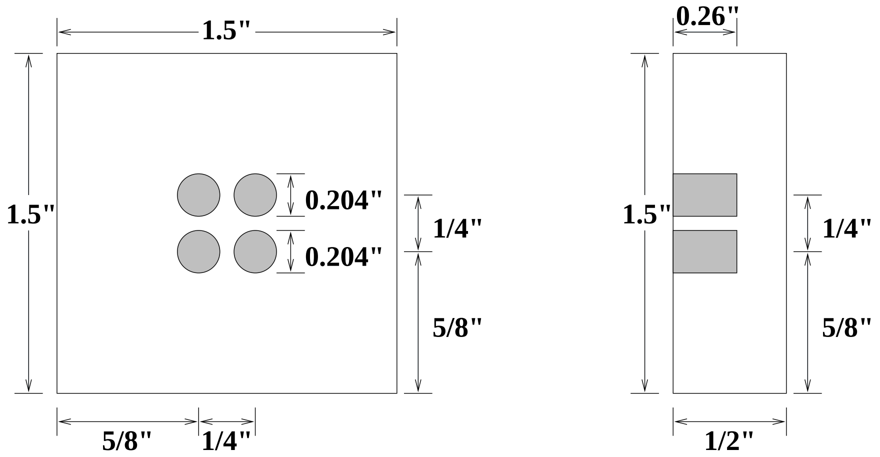

Fig. 7. LED Block Dimensions

In order to ensure the relative stability and uniform luminosity of the LEDs within an LED Block, the LEDs were prematched so that each draws the same current while delivering similar luminosities.

The LEDs are potted in an acrylic block using Bicron 600 Optical glue[7]. Since the intent is to distribute the light to the PMTs uniformly, the potting acts to remove the lensing effect of the LED casing by taking advantage of the similar indices of refraction of the LED casing, glue, and lucite.

Two types of LED blocks are used in the system. They are differentiated by the type of LED potted in the block. In the central region, Blue-Green NSPE510S LEDs from Nichia America Corporation[8] are used since the peak wavelength and shape of their emission spectrum best matches that of the wavelength shifting fibers used in the counters, Fig. 8(a). In the forward regions, Blue NSPB320BS LEDs from Nichia America Corporation are used since the peak wavelength and shape emission spectrum best matches that of the wavelength shifting bar used in the pixel counters, Fig. 8(b).

2.4 Light Mixing

The light is further mixed in two additional lucite mixing blocks. The upstream side of each block is frosted by sand-blasting the lucite with a high powered silica bead blaster. The sides of the block are polished to maximize total internal reflection within the remainder of the block.

The first mixing block is used both to mix the light, to physically separate the PIN diode/OpAmp from signals induced by the LDB pulses, and to provide

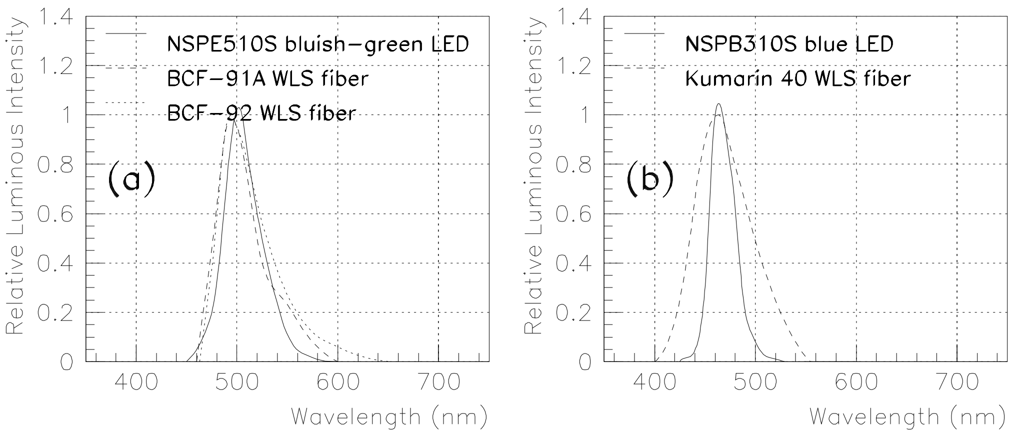

Fig. 8. Emission Spectra for WLS fibers, bar, blue LEDs, and blue–green LEDs

a surface from which the PIN diode can collect light. The dimensions of the first *(upstream)* mixing block are $1.5'' \times 1.875'' \times 3.325''$. The dimensions of the second *(downstream)* mixing block are $1.5'' \times 1.5'' \times 2.85''$. Note that the first mixing block is larger than the second mixing block by $3/8''$ in one transverse dimension so as to accommodate the PIN diode. The second mixing block is square in cross section and serves to further mix the light using total internal reflection and by taking advantage of the optimal aspect ratio of $length = 1.9 \times width$[9]. Both mixing blocks were polished using a diamond cutter.

2.5 Light Distribution

Each LMB serves to pulse numerous PMTs by distributing the mixed light to individual PMTs via Hewlett Packard HFBR-500[10] clear optical fiber cable. A lucite block, into which these fibers are glued, has the same transverse dimensions as the second mixing block, as shown in Fig. 9. This block, with fibers inserted, is referred to as the *fiber block*. Within each fiber block, the length of each fiber is identical.

In order to minimize the cost of the project, it was important to reduce the amount of optical fiber used. We used arrays of 3×3, 4×4, 4×5, 5×5, 6×6, 7×8, 8×9, or 10×10 fibers in a block to adapt to the different counter geometries. In doing so, we also required that: (1) fiber lengths ≤ 7 m, (2) radius of curvature for each fiber ≥ 35 mm, and (3) each block had a minimum of 5% spare fibers.

Due to the variety of counter types in the central region, a total of 36 LMBs of each flavor is installed to serve the 1,350 CMSC PMTs. In the forward regions, a single 10×10 LMB is installed in each octant of each plane of counters for a total of 48 LMBs to serve the 4608 FMSC PMTs.

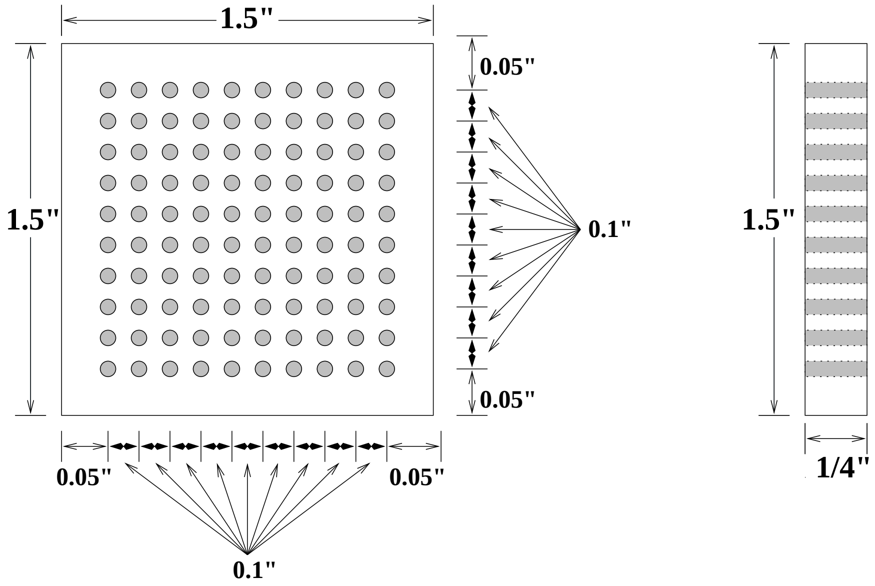

Fig. 9. Fiber Block Dimensions

Once all of the fibers are potted in the fiber block, the fibers are back–filled with a black epoxy, as shown in Fig. 4. The back–filling serves to both strain relieve the fibers and to form a light–tight barrier for the back piece of the housing, see Sec. 2.9.

2.6 Connection to PMTs

At the end of each fiber from a fiber block is a Hewlett Packard HFBR-4501B[10] black simplex connector. Butted up to each PMT is a polished piece of fiber with the black simplex connector on the other end; the connector end of the fiber is then plugged into a black bulkhead connector, Hewlett Packard HFBR-4505B[10]. Coupling between the LMB fibers and PMT fibers is made with the bulkhead connector.

In the CMSC system, the unconnected fiber end is glued into a hole drilled into a lucite cookie[3]; the other end of the fiber is connected to a bulkhead connector in the counter PMT cover. In the FMSC system, 87 mm long fibers with polished ends are taped to the wave–length shifting bars which mate to the PMTs; the other end of the fiber is fed through a hole, which is subsequently filled with RTV, and coupled to a bulkhead connector mounted on the counter chassis.

In the FMSC counters, light transmission variations of $\pm 7\%$ were observed in the fibers between the PMTs and bulkhead connectors. Since the difference

[3] The cookie is designed to hold all of the scintillator fibers to the face of the PMT.

between FMSC and CMSC pieces are minimal, the same variations in light transmission are expected in the CMSC system.

2.7 LED Pulser System Monitoring

The bench tests of mixing blocks show that the light is distributed homogeneously to the fibers, Sec. 3.3. Consequently, we can monitor the light with a PIN diode at the downstream end of the first mixing block, and use this to track the light intensity for all of the fibers in the LMB over extended time periods.

Knowledge of the light intensity from the LEDs allows for the decoupling of any variations of the LEDs from that of the phototubes. This is accomplished by taking the ratio of the amplitude of LED light from the PMT, $\mathcal{A}_{PMT}$, to the amplitude as detected by the PIN diode, $\mathcal{A}_{PIN}$. Assuming that the PIN diode is stable over time, this ratio is independent of the intensity of light from the LEDs over time.

Upon commissioning of the LED Pulser System, the ratios were measured for each PMT and stored in a database. During operation, the ratios are periodically measured and compared to the values taken at commissioning. If the ratio has drifted by 10%, the channel will be flagged as unstable, and the operator is notified by the online system so that action may be taken.

2.8 PIN PhotoDiode and Amplifier

To monitor the light from the LEDs, we use Hamamatsu S6775 Silicon PIN photodiodes[11]. The photodiode is operated at a reverse voltage of 6 V and the output current is converted and amplified by a charge sensitive preamplifier, or *CSP*, as shown in Fig 10. The CSPs were taken from the electronics used in Run I to read out the cathode pads of the DØ muon proportional drift tubes[12]. The output from the CSP is amplified by a factor of 40 by a OPA650 operational amplifier and a MAX435 transconductor. The combined system, Fig. 11, converts 70k photons, or a 7.1 fC signal, from the photodiode to a 100 mV output signal at the amplifier. The power requirements are 7 mA at -12 V and 12 mA at +6 V for a total of 156 mW. We refer to the combined PIN diode and amplifier circuitry as a PIN/Amp.

We use three flavors of PIN/Amps to match the two types of LEDs used. The gain differences are set by the resistors at U3, see Fig. 11: the blue PIN/Amps use 200Ω resistors for a 1× gain, the green PIN/Amps use 100Ω and 50Ω

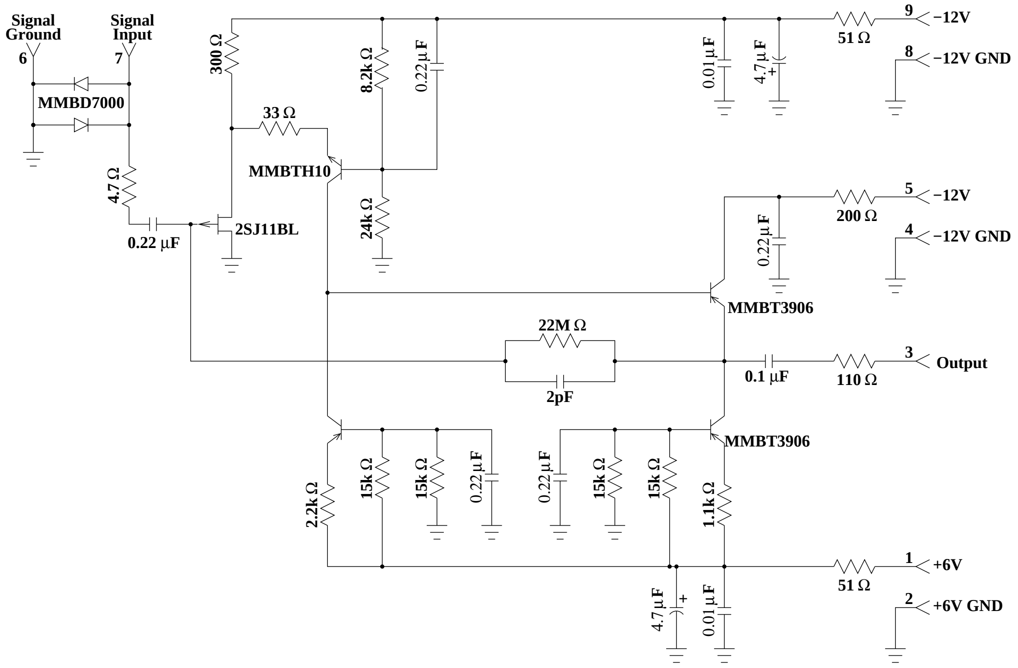

Fig. 10. D0 Charge Sensitive Preamp: CSP

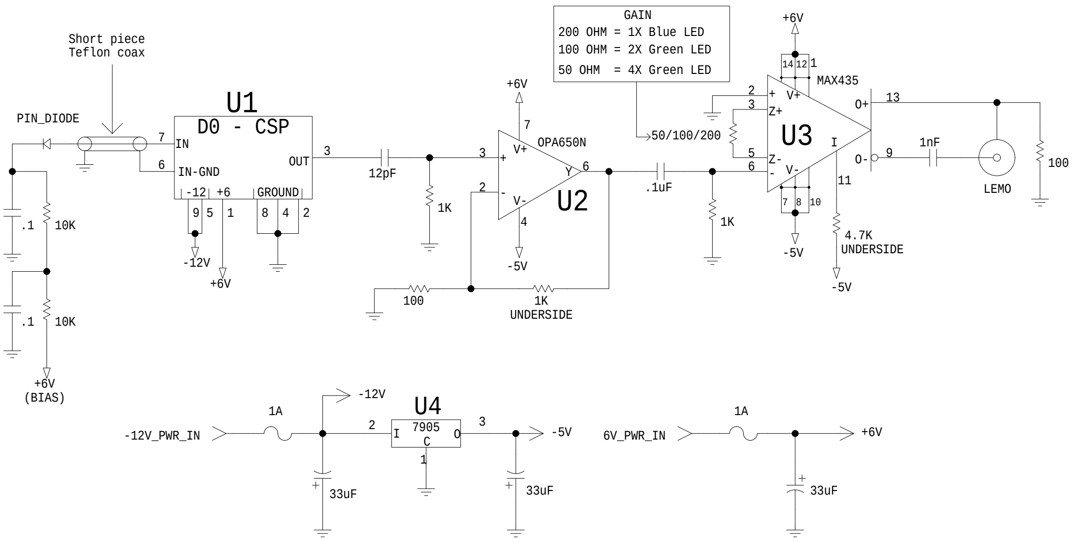

Fig. 11. Amplifier Circuit Diagram for PIN Diode

resistors for 2× and 4× the amplification as the blues. This choice maximizes the use of the dynamic range of the SFEs.[4]

[4] The different green LMBs are used in different parts of the CMSC system.

On the front piece of the LMB housing a 5 pin male WPI126-223 WPI connector[13] is installed for the PIN/Amp power leads. On the inside of the LMB front piece, three wires are soldered for +6V, -12V, and ground to Molex 1560 and 03062032 male terminal pins and socket[14]. These power leads connect to Molex 1561 and 03061032 female terminal pins and receptacle which connect to the power leads which supply the PIN/Amp circuit. Due to the possibility that the long leads from the power supply source to the LMB may pick up noise from the VME switching power supplies or the 1553 protocol, the leads are wrapped 7 times around a T22/14/6.4-3E2A ferrite core[15], see Sec. 3.8.

The signal from the PIN/Amp is returned on an RG174-U coaxial cable to a BNC/lemo bulkhead connector mounted on the LMB front piece. An RG58-U cable returns the signal to the muon readout electronics.

2.9 LMB Housing

The LMB housing is designed to house the LMB components in a secure, safe, and light-tight unit. The material chosen to construct the boxes was black linen phenolic. Though messy in terms of dust when machining, the black phenolic is relatively easy to machine, strong, light–tight, and non-conductive.[5] The box pieces were individually routed to create baffles to insure light–tightness. The pieces were then drilled, tapped, and countersunk.

The base and top pieces are routed such that an outer square channel serves as the baffle for the front, back, and side pieces. A central channel in the base provides a slot for the LMB optical parts. A step in the base central channel serves to guide the back–filled part of the fiber block. A widened part of the top central channel serves as space for the PIN/Amp box. These central channels can be seen in Fig. 4.

The front piece houses the BNC/lemo bulkhead connectors for the input of the SLP signals and the PIN Output, as well as the power connector for the PIN/Amp. Four tapped through holes in the back piece are used for screws which provide compression for LMB parts. The bottom two screws push a collar which rests on the fiber block back–filled section and compresses all LMB optical pieces together against the front ridge in the base central channel where the LED block is positioned. This keeps all of the optical pieces secure within the box. The top two screws are used to push the PIN/Amp box against the first mixing block.

[5] Black plastic would have been a good choice for material for the box. However, though an exhaustive search was not made, our first choice of black plastic was rejected since it was translucent when milled down to 1/8" thickness.

To assemble the box, all three connectors are installed on the front piece. The front and side pieces are then glued and screwed together onto the base. The optical parts are then installed in the box, and the back–filled part of the fiber block is sealed with black RTV. As the back and top pieces are designed to be removable, they are not glued into the baffles. These are then screwed into position, and the back piece compression screws are moderately tightened.

3 Light Mixing and Pulser Stability Test Results

3.1 LED Robustness

In the muon system we operate the LMB at 178 Hz. Therefore to observe the LED's behavior over the course of Run II, we pulsed a single LED with 30 mA pulses with a duration of 30 ns at a rate of 1.5 kHz for 5,283 minutes (3.7 days). The LED Pulser System is operated for ∼4 hours/week. This corresponds to about 3.6 years of running, and is equivalent to a total integrated current of 0.014 C. The luminosity vs time dependence was measured by setting the driving voltage of the SLP such that the LED yielded a specified amount of light as measured by the PIN diode. Using the voltage drop across an LED–resistor leg as a measure of the change in luminosity, the long term stability of the LED is shown in Fig. 12.

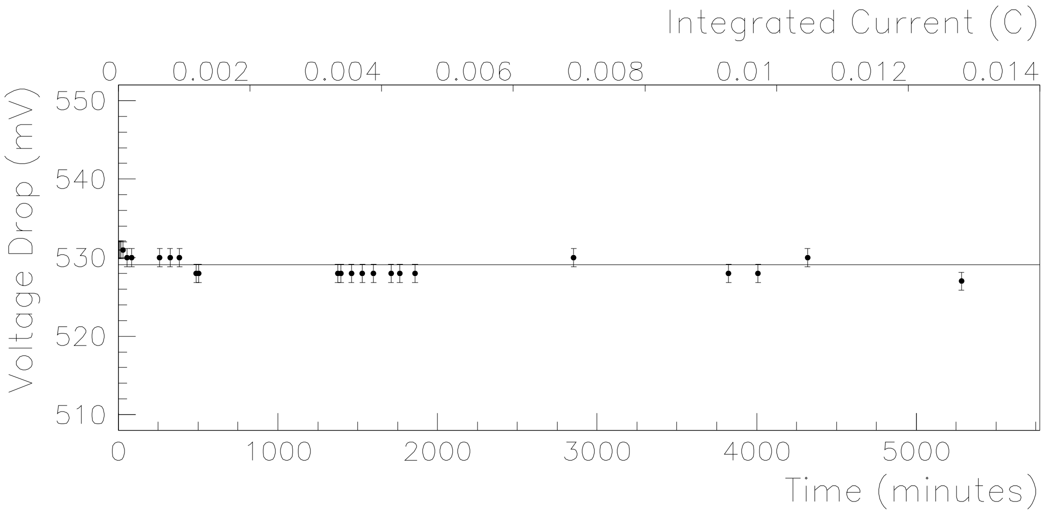

Fig. 12. LED Luminosity vs Time and Integrated Current

The voltage required to drive at the reference luminosity fluctuated ±0.02 V (±0.4%) through out the study. Considering the measurement errors, the luminosity variations of the LED are consistent with a stable LED for the integrated current used in our measurement.

In addition, our tests show that the Nichia LED's do not have a burn in period.

LED Current Limitations

According to the manufacturer specifications, Nichia LEDs should not be driven with currents larger than 100 mA. Currents exceeding the manufacturer's specifications can have two possible effects: that the LED ceases to operate, or that the high current may change the LED's characteristics, such as the luminosity—voltage dependence.

In the event of a malfunction in the circuit in which the current may reach a level that exceeds the Nichea's specifications, tests were performed to push the limits. Pulsing a single LED at 1.5 kHz with currents up to 188 mA revealed that the LED did not die and the $\mathcal{L}$—vs—V dependence did not change.

Additional tests were made to measure the current through a single LED leg in the LDB. Even with the SLP driving at 10 V, the current through any LED was <50 mA. We conclude that even if the SLP and LDB circuits malfunction, the LEDs will not fail from being operated out of the range of the manufacturer's specifications.

3.2 LED Matching

A primary concern for light mixing is that all 4 LED's in an LED Block yield the same luminosity, $\mathcal{L}$, to within 10%. Since LEDs are inherently non-linear devices, it is equally important that the luminosity is attained by driving all four LEDs with the same current. This motivates an interest in the long term stability of the LEDs to insure that they do not change characteristics over time or integrated current. A second concern is that if the LEDs are matched at one point in their $\mathcal{L}$—vs—V or $\mathcal{L}$—vs—I curves, will they still be matched at another operating point?

As previously mentioned, LEDs are prematched before being potted into the LED block. To verify that matching the LEDs at one point along the $\mathcal{L}$—vs—V curve would not result in mis–matched LEDs operated at another point, 3 bluish–green and 3 blue *unmatched* LEDs $\mathcal{L}$—vs—V curves were measured. The curves are shown in Fig. 13, where different polymarkers represent different LEDs.

To better see whether the LEDs match, the two lower current curves in each plot in Fig. 13 were scaled to match the higher current curves and replotted in Fig. 14. From the plots, one can predict that as long as matched LEDs are

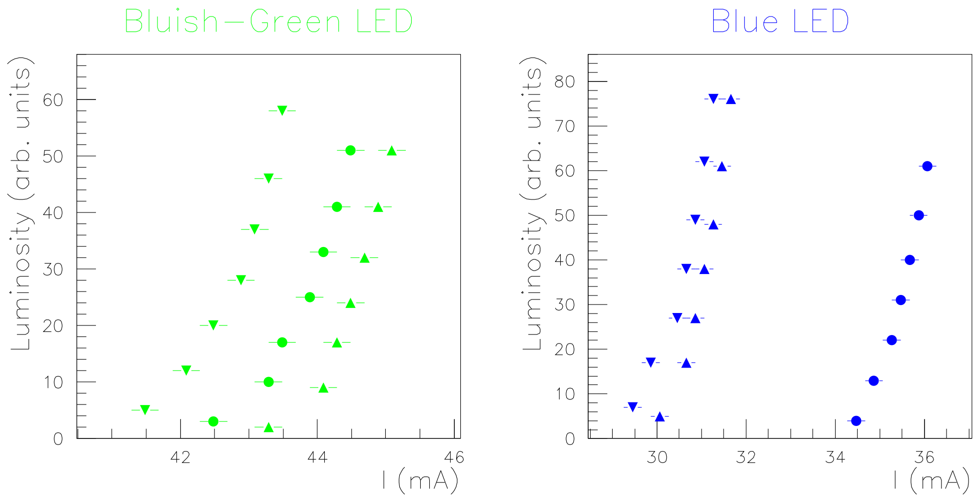

Fig. 13. $\mathcal{L}$—vs—I curves for Nichia bluish–green and blue LEDs; different symbols correspond to different LEDs

operated within a stable region, i.e. high enough on the $\mathcal{L}$—vs—V curve, they will remain matched over the range of operation.

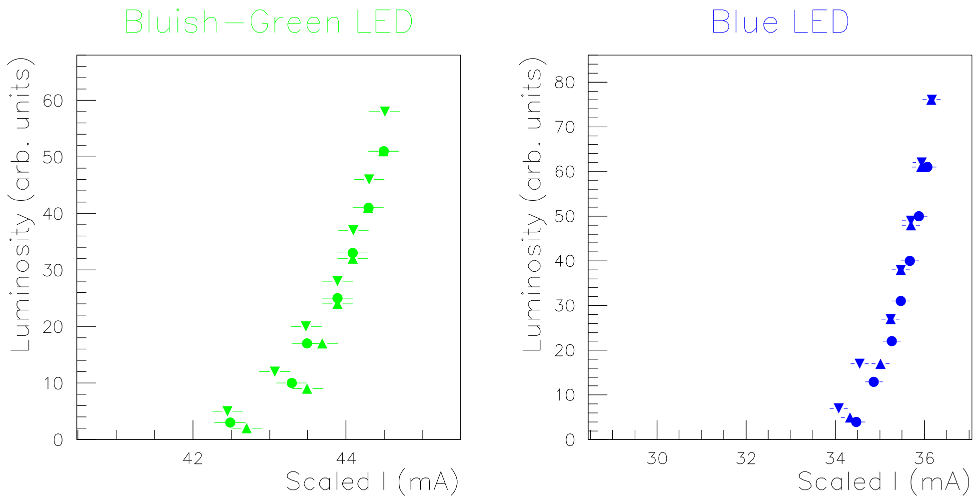

Fig. 14. $\mathcal{L}$—vs—I curves with currents scaled for Nichia bluish–green and blue LEDs; different symbols correspond to different LEDs

3.3 Light Mixing Uniformity

In order to study how homogeneously the light is mixed in the combination of LED block, first and second mixing blocks, a blank fiber block was mounted in the LMB box. In each of the 100 holes of the blank fiber block, a fiber which was attached to a PMT was inserted. For each point both the PMT and PIN Diode outputs were recorded using a LeCroy 3001 qVt in integrated charge mode.

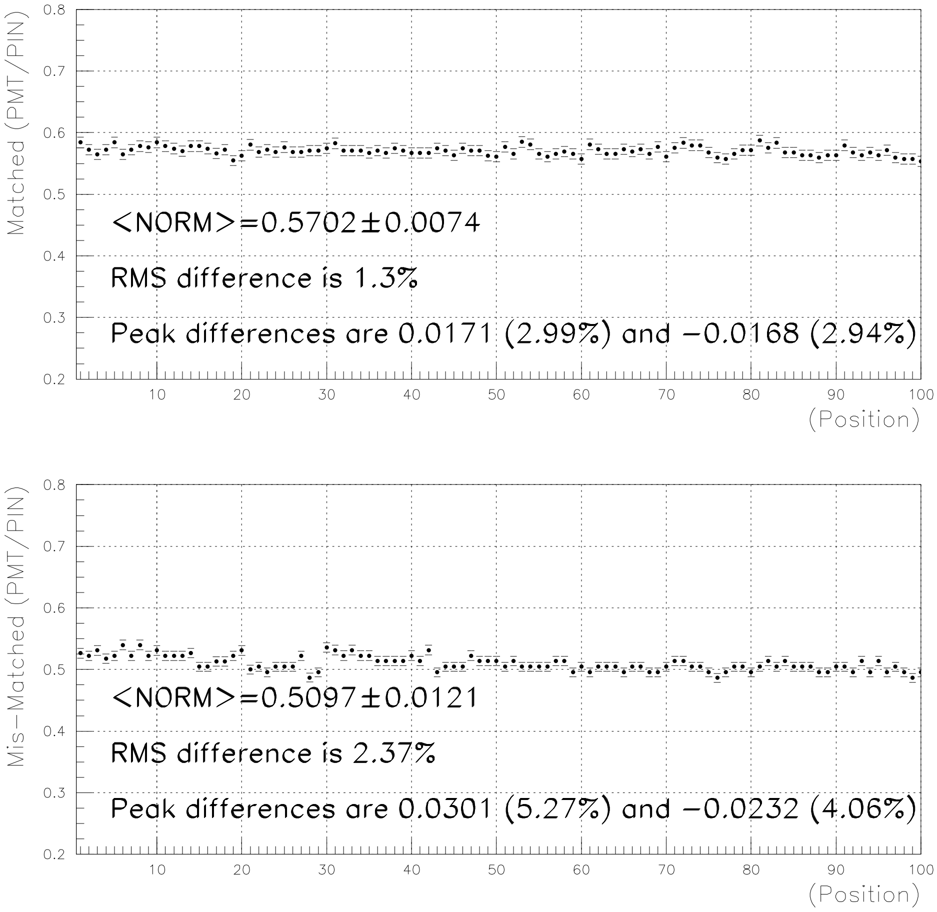

Fig. 15. LMB Light Mixing Uniformity after the LED block and two mixing blocks: the top plot uses matched LEDs, the bottom uses mis–matched LEDs in the LED block

Fig 15 shows the peak ADC counts as seen by the PMT/PIN Diode ratio for each position as measured by a single fiber in a 10×10 array after the light has been mixed. In the plot, the first ten points correspond to the first row of ten fiber block holes, the second ten points to the second row, etc. The top plot, using matched LEDs, shows that the RMS difference from position to position is 1.3% with a maximum variation of 3%. In the bottom plot, mis–matched LEDs [6] were used which resulted in a 2.4% RMS difference with maximum variations of 5.3%. From the figure, it is clear that matched LEDs improve light mixing.

In order to ensure that we did not misinterpret our results, we tested for the

[6] The green LEDs were mis–matched in light output by up to 5% and the blue LEDs by up to 14%

possibility of a conspiracy of a single hot LED and poor transmission in the fibers which point to it. This test was performed by rotating an LED block in 90 degree increments with respect to the mixing blocks and fiber block and measuring the light yield from several fibers at each position. The comparisons confirmed that the light is mixed by yielding the same amount of light in any orientation of the LED block.

In conclusion, the LED block and two mixing blocks perform well the task of mixing the light. Mixing is improved when the LEDs are matched within the LED block.

3.4 Light Distribution to PMTs

At this point along the optical path from the LEDs to the PMTs, the light is mixed homogeneously as shown in Sec. 3.3. The light is then distributed to the PMTs from the fibers in the fiber block. The concerns become (1) consistancy in polishing fibers for light transmission, (2) light loss at optical fiber couplers, (3) consistency in mating optical fiber couplers, and (4) homogeneity of light distribution.

3.4.1 Fiber Polishing

A series of tests were performed to compare various fiber polishing techniques; details of the tests can be found in DØNote 3561[16]. We chose a method known as "ice polishing", in which numerous fibers are bundled together and frozen to keep them solidly positioned with respect to each other. While still frozen, the bundle end was polished using a diamond cutter.

Light Loss in Optical Fiber Couplers

As described in Section 2.6, the fibers are coupled together using Hewlett Packard HFBR-4501B simplex connectors and HFBR-4505B bulkhead connectors [7]. Several factors contribute to the loss of light at the couplings: (1) misalignment of the two simplex connectors within the bulkhead connector, (2) the fiber protrudes or is retracted from making a flush surface with the end of the simplex connector, and (3) fiber is bent with too small a radius close to the connector.

Light loss due to misalignment of the fibers within the bulkhead connector is

[7] The "B" refers to black. In our tests, however, we found no significant differences in performance between gray and black connectors.

dominated by geometric effects. Since the fiber, and associated connectors, are not designed for single photon counting, the connectors are not designed to have strict tolerances. Despite this, the couplers are fairly reliable. If the fiber protrudes from the end of the connector, it is possible that it will displace the fiber entered from the other end causing a misalignment of fibers. On the other hand, losses also occur if the fiber is retracted from the connector end; for a gap of $\gtrsim$ 0.3 mm, we measured a $\geq$10% loss of signal.

Though the manufacture specifies a minimum radius of curvature of 3.5 cm, Section 2.5, we have found that a radius of curvature of <15 cm near the fiber coupler results in significant losses.

Superior methods of coupling two optical fibers exist, though they would likely come at a higher price than the Hewlett Packard couplers. Our measurements yielded a transmission rate of $80 \pm 1.5\%$ under optimal conditions.

3.4.2 Light Distribution Results

Given that the light is well mixed up to the fiber block, see Sec. 3.3, one can measure how homogeneously the fibers distribute the light to the PMTs.

To perform this measurement, a single pixel counter was used and operated at the nominal HV. A complete LMB was used in which each fiber was connected one–by–one to the PMT. Simultaneous readings of the PMT output and PIN Diode output were recorded. The ratios of the PMT outputs to the PIN Diode output for each fiber are plotted in Fig. 16.

3.5 LMB Stability

Fig. 17 shows the stability of the LED Pulser System over an 89 day period. During that period, individual runs at a test stand were taken which consisted of 16 separate measurements per run. Data were taken in which a single counter was triggered by cosmic rays and LED triggers from a prototype LED Pulser System. For each measurement of each run, $\sim$500 cosmic ray triggers and $\sim$1300 LED triggers were accumulated.

Fig. 17 shows the average of each of the 16 measurements of each run plotted for both the cosmic ray triggers and the PMT/PIN ratio of LED triggers; the PMT/PIN ratio points are normalized to fit the plot scale. Here the top points are the cosmic ray triggers, and a solid line is fit to the resulting points. The slope shows that the PMT's gain has dropped $\sim 4\%$ over the course of the tests. The PMT/PIN ratio points are plotted below the cosmic points, and a dashed line is fit to these points. For comparison, this fit line is replotted as a

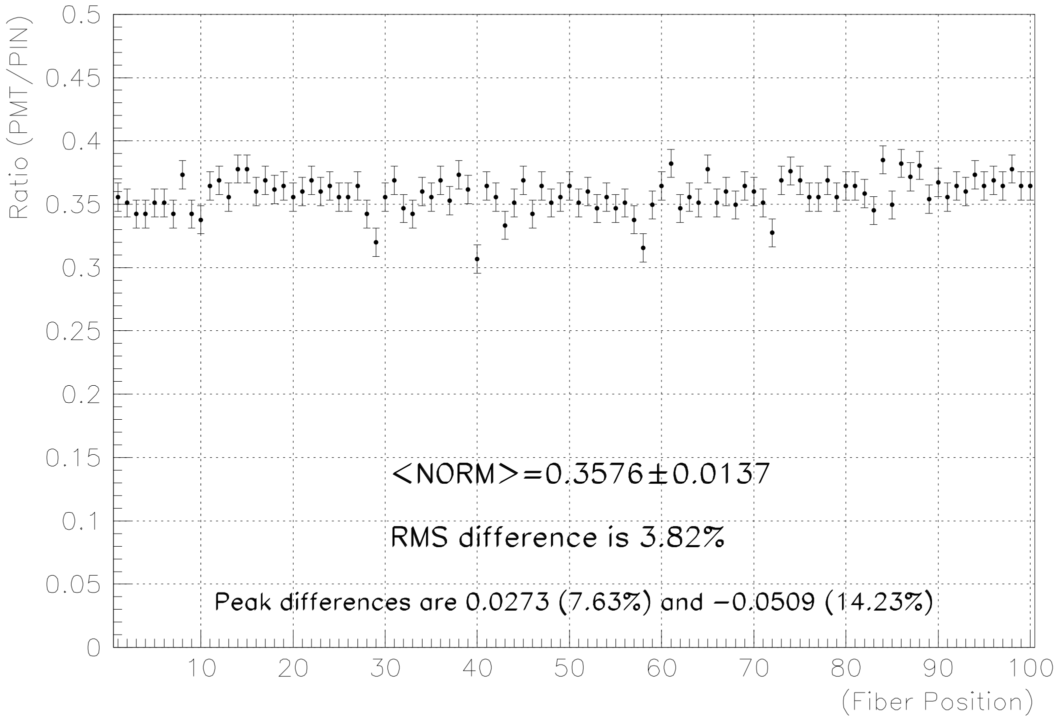

Fig. 16. Light Distribution Uniformity at fiber ends of LMB

dotted line using the cosmic fit's line y–intercept. Analysis of the fits reveals a 4% drift in gain of the PMT. As can be seen in Fig. 17, a comparison with the slope of the ratio fit yields that the LED Pulser System tracks the PMT gain by $\sim$0.2% over the 3 month period. Due to the large statisitcal sample, the error bars are smaller than the points.

Note the scatter in the PMT gain for both cosmic and LED triggers as shown in Fig. 17. Fig. 18 shows a ratio of the cosmic ray triggers to the ratio of normalized PMT/PIN ratio of LED triggers. This shows how well the LED Pulser System can be used to track gain changes in the PMTs, as one can clearly see that the ratio points lie in a straight line, and the slope of this line is 10^{-7}. The rms variation is about 0.7% for each point.

The fit results show that the LED Pulser System is capable of performing the task of monitoring the muon counter PMTs well within the 10% specification.

3.6 System Stability Against Supply Voltage Variations

Since the PIN/Amp is used to monitor the performance of the LED Pulser System , it is important to know the range of operation in which it will be stable. Two of these parameters are the operating and bias voltages.

The PIN Diode amplitude was measured as each of the supply voltages was varied. It was found that a 1% stability in the PIN Diode amplitude requires

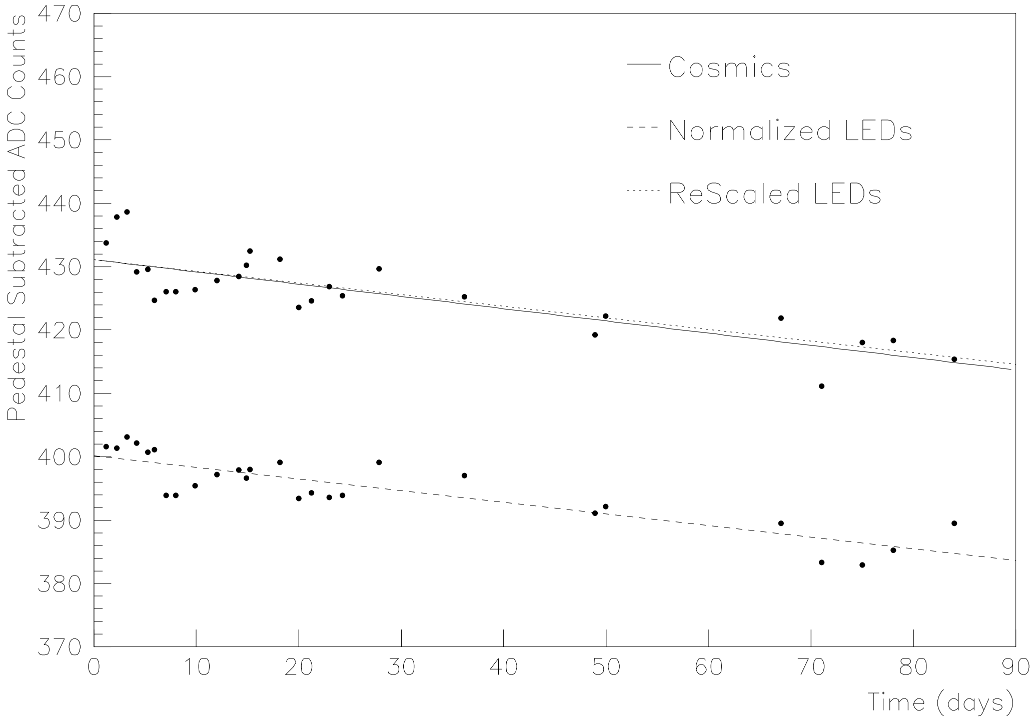

Fig. 17. PMT gain drift as tracked by LED Pulser System

that the -12 V supply voltage must be stable to within ±0.33 V, while it is sufficient for the +6 V supply be stable to within ±0.58 V.

3.7 System Stability Against Temperature Variations

Though the DØ collision hall is kept at 20.6±1.1°C, one expects local fluctuations in temperature. As high temperatures may affect the electronics, we tested an LMB in an oven and measured its performance as a function of temperature. Knowing that the phenolic housing is a fairly good insulator, we used temperature probes both within the oven and within the LMB housing.

In order to test the stability of the calibration system under temperature changes, an LMB was operated in a temperature-controlled oven with one of the optical fibers running outside of the oven to a PMT which was at room temperature. It was pulsed at a constant DC offset while the temperature was varied, and the amplitudes of both the PMT signal and the PIN signal were monitored as a function of the temperature inside the LMB housing. The PMT signal varies by 0.8%/°C, while the ratio of PMT to PIN varies by only

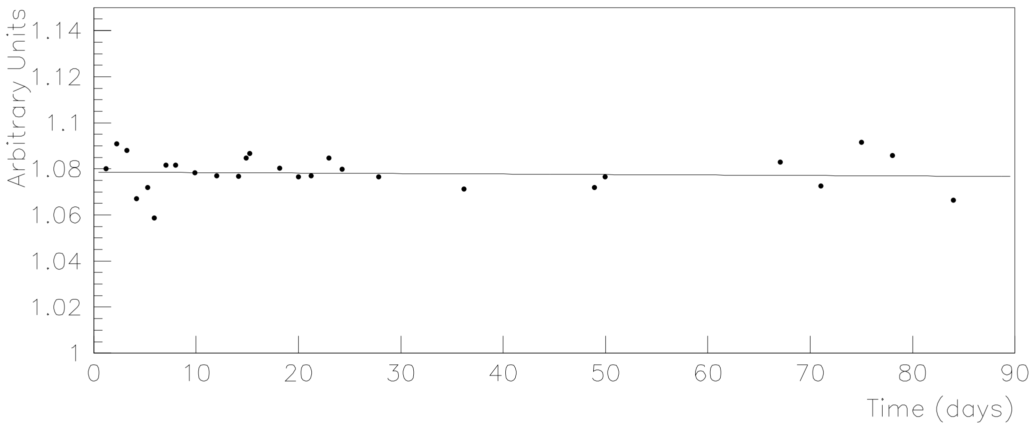

Fig. 18. Ratio of cosmic to PMT/PIN LED triggers as tracked by LED Pulser System

-0.2%/°C. Therefore, in order to maintain a stability of 1% in the ratio, the temperature must not vary by more than 5°C.

The temperature variation of the short circuit current for the PIN photodiode is of the order of 0.02%/°C[11]. So the variation measured for the LMB is due mainly to the temperature variation of the PIN photodiode amplifier and LED output variations with temperature.

The electronics inside of the LMB housing generate heat. With an ambient temperature of 20°C, the interior of the LMB stabilizes at about 34°C. On first turning on, the LMB requires approximately one hour to heat to within 5°C of its asymptotic temperature. For maximum stability, the LMBs are normally powered on, and are not used for precision measurements for the first hour after having been powered off.

3.8 System Stability In a Noisy Environment

The DØ detector has numerous switching devices that radiate noise which could be picked up and affect the operation of the LMB. The noise sources are from the VME switching power supplies and 1 MHz from the 1553 protocol system. Since the PIN/Amp is enclosed in a copper box which serves as a Faraday cage, our concern is only for the 1 MHz signals through the holes. However, both sources can be picked up in the PIN/Amp power leads. Hence, we use the ferrite core to protect the power leads, see Sec. 2.8.

Using an oscilloscope, and measuring the noise near a 1553 source as well as the output of the PIN/Amp, we observed a 3 mV ripple when the LMB was within 10 cm of the crate. Since we would never mount the LMBs this close to the crates, we concluded that the noise problem from this source is negligible.

3.9 System Stability In Magnetic Fields

Two separate tests were made to search for instabilities in the PIN/Amp when it was placed in a magnetic field. There is no theoretical reason that the LDB or PIN diodes would be affected, but the ferrite core around which the PIN/Amp's power leads were wrapped might saturate depending on the orientation with respect to the magnetic field.

The first test was performed by placing an LMB in a permanent magnetic dipole with a maximum field of 400G. The LMB was rotated in three different orientations and positions so that each axis of the box was parallel to the magnetic field. The field was measured with a Hall probe. In this measurement, there was no noticeable change in the noise level of the PIN/Amp output up to a field of 300G.

In the second test, an LMB was mounted in the DØ detector in a region calculated to have fringe fields between 250 and 300 G from both the solenoid and toroid magnets. A PMT was placed outside of the magnetic field region, $\mathcal{O}(1\text{ G})$, and a long optical fiber was routed from the LMB to the PMT. The light from the LMB was measured in both the PMT and PIN/Amp with the magnetic fields on and off. Pulsing the LMB at 3 kHz, the pulse height from the PMT was measured using the averaged output from a digital scope. The pulse height was unchanged with the magnet on and off.

Since the expectation was that the PIN/Amp might be affected by magnetic fields, magnet on/off tests were performed at different driving voltages and the pulse shape was recorded. The results are shown in Tab. 1. From the table, it is clear that within measurement errors, the LMB is not affected by magnetic fields of up to 300 G [8].

4 System Control

Communication with the SLP are via VME commands generated by the 68k controller/crate master within the crate. Commands consist of setting regis-

[8] The 300 G fringe field is considered to be a region of maximal magnetic fringe field which is a worst case scenario for positioning an LMB.

V_{SLP} (V)	V_{peak} (mV)		t_{rise} (ns)		t_{fall} (ns)		t_{fwhm} (ns)	
Magnet	off	on	off	on	off	on	off	on
7.5	5.5	5.3	33.5	35.0	115.0	117.0	82.5	86.5
8.0	23.7	23.7	37.0	37.0	152.5	154.0	85.5	85.5
8.5	61.6	61.2	37.5	38.0	130.5	143.0	87.0	87.5
9.0	119.6	118.8	37.0	37.5	128.5	135.5	87.0	87.5
9.5	194.0	195.0	37.0	37.0	122.5	124.5	86.5	87.0
10.0	276.0	276.0	37.0	37.5	121.0	124.0	86.5	86.5
8.5	61.2	61.2	37.5	37.5	132.5	137.5	87.5	87.5

Table 1
Comparison of effects of Magnet On/Magnet Off studies on PIN/Amp

ters which control the DACs and Enable Registers within the SLP. The 68k controller is addressed using the standard 1553 interface, or through the RS232 console port.

The tasks performed with the LED Pulser System include: (1) test functionality of the PMTs, (2) test for gain stability of the PMTs, (3) test linearity of PMTs, (4) scan gates, and (5) decouple front end electronics from PMTs by pulsing the system with no light to the PMTs.

A block diagram of the SLP control is shown in Fig. 19.

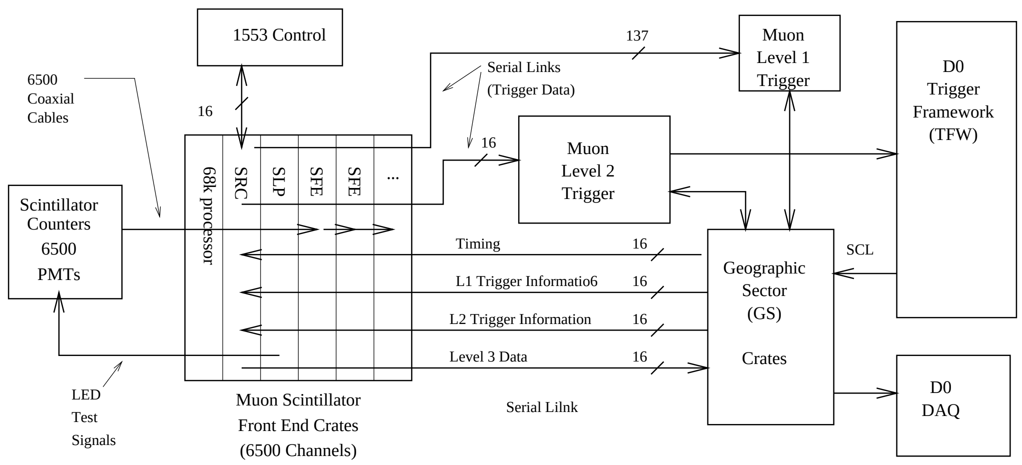

Fig. 19. Driving circuit for single SLP channel

5 Experience with the LED Pulser System

5.1 Test Stand Results

Monitoring the PMT/PIN ratio gives good handle on relative change in PMT gain, or equvalently, the photo–electron yield of the PMT. However, this ratio depends upon the intensity of light, which in turn depends on the LEDs, light mixing, light distribution, and fiber length; in short, it depends on which actual LMB was used. Since the LMBs on the DØ detector are different from that used in testing the CMSC counters in the cosmic ray teststand prior to installation, data from the teststand cannot be directly used in monitoring of the relative PMT gain changes in Run II. Therefore, we need to monitor the absolute gain of each PMT independently of which LMB is used.

We determined the gain of the PMTs using LED data taken in 1998 at the CMSC teststand using the prototype LED calibration system. The gain is also determined at regular intervals during Run II. These data are then cross–calibrated and used for monitoring each PMT gain.

For each PMT, the gain can be determined using the signal and pedestal charge distributions of PMT and PIN signals at different PMT high voltages. The PIN data is used to normalize small fluctuations (if any) in the LED intensity during the calibration run. Though, we can not correct for fluctuations on an event by event basis due the finite width of the pedestal distribution, the PIN data can provide, on average, an overall correction to any LED intensity fluctuations. Using the charge distribution data from the PMT and PIN, we first determine the photo–electron yield, which is then used to determine the gain using the ADC calibration constant. We can show[18] that the number of photo–electrons ($<p.e.>$) is:

$$<p.e.>= \left[\left(\frac{\sigma_{PMT}}{<PMT>} \right)^2 - \left(\frac{\sigma_{PIN}}{<PIN>} \right)^2 \right]^{-1} \tag{1}$$

where

$$<PMT> = <PMT_{PH}> - <PMT_{PED}> \tag{2}$$
$$<PIN> = <PIN_{PH}> - <PIN_{PED}> \tag{3}$$
$$\sigma_{PMT} = \sqrt{\sigma^2_{PMT}(PH) - \sigma^2_{PMT}(PED)} \tag{4}$$
$$\sigma_{PIN} = \sqrt{\sigma^2_{PIN}(PH) - \sigma^2_{PIN}(PED)}. \tag{5}$$

Here, “PH” refers to Pulse Height and “PED” refers to Pedestal value.

$< PMT_{PH} >, < PMT_{PED} >, \sigma_{PMT}(PH), \sigma_{PMT}(PED), < PIN_{PH} >, < PIN_{PED} >$, $\sigma_{PIN}(PH)$, and $\sigma_{PIN}(PED)$ are fitted parameters determined from their respective charge distributions. A typical charge distribution and fitted parameters for PMT signals with LED triggers is shown in Fig. 20.

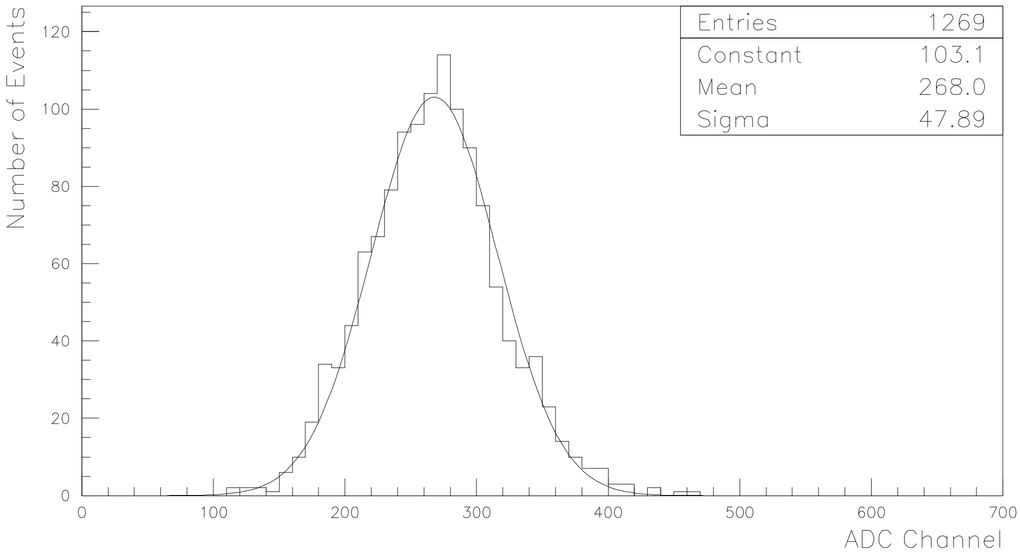

Fig. 20. Typical ADC distribution for a PMT

The sensitivity of the photo–electron determination method can be studied by obtaining the photo–electron yields at fixed LED intensity with different PMT high voltages. Since the LED intensity is fixed, the photo–electron yield is expected to remain same at each of these voltages. Data was taken at 6 different voltage settings for each of 6 PMTs. The ratio of the photo–electron yield to the mean yield is plotted in Fig. 21. It can be seen that we can determine the yield to the accuracy of less than 7%.

Once the photo–electron yield is determined, then the gain, G_{PMT}, of the PMT can be determined using the ADC calibration constant ADC_{CAL}:

$$G_{PMT} = \frac{ADC_{CAL} * < PMT >}{< p.e. >} \tag{6}$$

There are 720 PMTs in the outer layers of the central muon detector. LED data taken for all PMTs in 1998 were used to determine the gain of each PMT at different high voltages. These data was interpolated to obtain the gain at the respective operating voltage. We shall refer this data set as *Teststand* data.

Fermilab's Run II began in 2001. Calibration data were taken during this period for the entire CMSC detector. The ratio of PMT gain during the beginning of Run II to the *Teststand* data is plotted in Fig. 22. It can be seen that most of the counters do not show any significant reduction in the gains

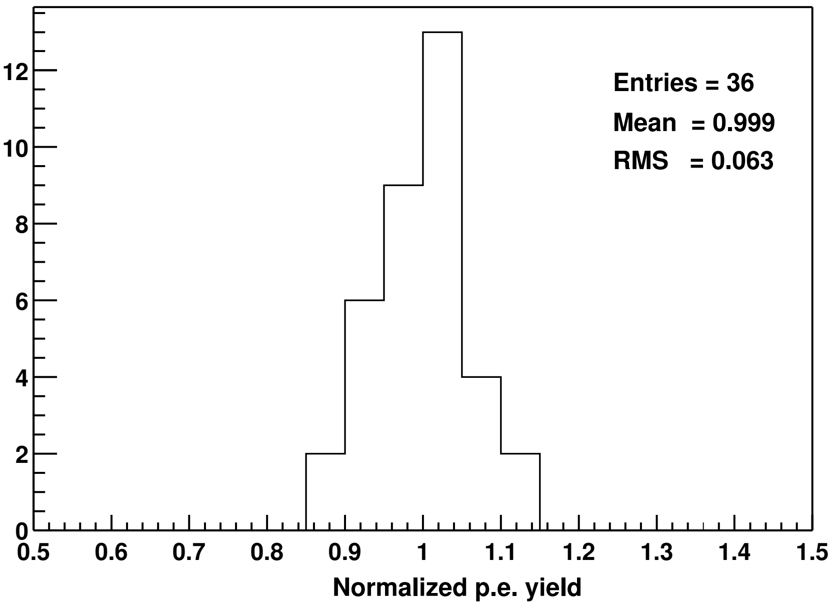

Fig. 21. Ratio of photo–electron yield at different high voltages to mean photo–electron yield.

of the PMTs. The width of the distribution is due to the resolution of p.e. yield estimation, uncertainty in ADC calibration constants, and interploation of gain vs. HV to obtain the gain at RunII operating voltages. Each of these contributes more or less equally to the width of ratio.

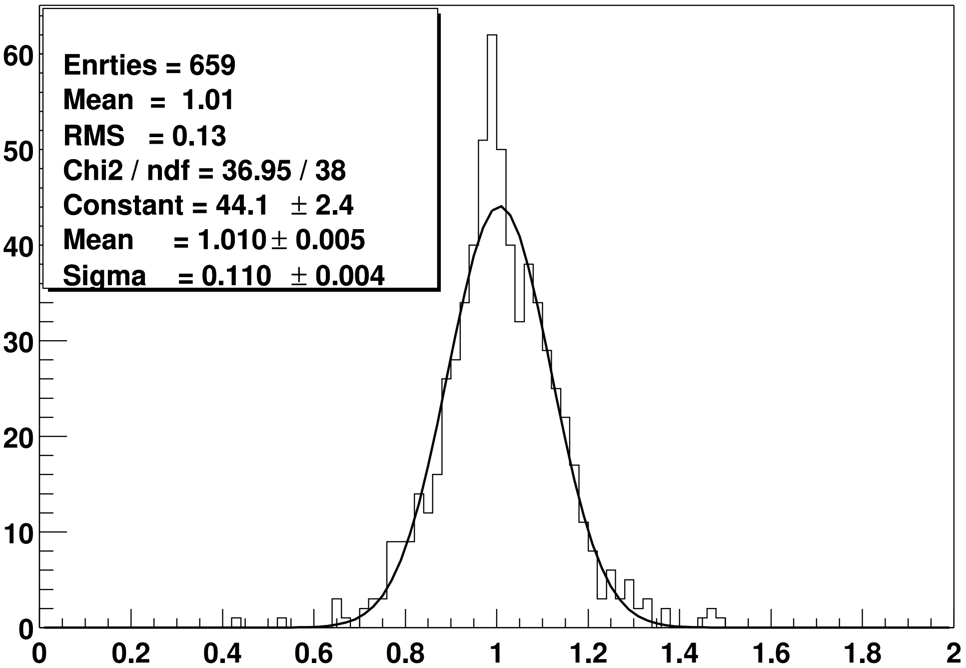

Fig. 22. PMT Gain Ratio of Run II/TestStatnd for B and C layers

The LED calibration system has been extremely useful not only in determining the gain of the PMT but also in setting discriminator thresholds which optimize the signal–to–noise level. The operating voltage for each PMT was determined from the cosmic muon *Teststand* data, which was obtained at a fixed discriminator threshold of 15 mV. However on the DØ detector, most of these PMTs are operating at different high voltages than those determined from the teststand. This is due to the grouping of 8 PMTs for each HV source. Hence, to optimize the signal–to–noise level, the discriminator thresholds should be determined for each PMT at their actual Run II operating voltages.

Also during the course of the run, if the gain of a PMT changes, then either the high voltage or the threshold has to be adjusted to maintain the detection efficiency of the counter and to minimize spurious noise. However, adjusting the high voltage is not feasible since this would alter the votages of the other PMTs that are in the same group. Therefore, we adjust the discriminator thresholds using the procedure described below.

We have determined the PMT gains at their respective operating voltages as described in Sec. 5.1. The threshold levels, $V_{th}(t)$, were then determined using,

$$V_{th}(t) = 15 * G_{PMT}(t)/G_{PMT}(t_0) \tag{7}$$

where, $G_{PMT}(t_0)$ is the gain of the PMT determined using *Teststand* data at the operating voltage and $G_{PMT}(t)$ is the current gain of the same PMT. The factor of 15 comes from the discriminator threshold used in the teststand.

The thresholds of all channels have been successfully set using this method.

6 Conclusion and Future Prospects

We have presented the description of an LED Pulser System of ∼5800 channels. The system delivers mip–like light signals which mimick the light from different types of scintillation counters in frequency, rise–time, and fall–time. The LED Pulser System has been a powerful and essential tool for the commissioning of these muon scintillation counters. During the data taking, it gives us a simple means to quickly locate malfunctioning PMTs, and determine gain and timing drifts due to the PMTs.

The LED Pulser System was used extensively during assembly and commissioning, and is now fully installed and operating in the Muon Scintillator System, and also the DØ Forward Proton Detector and the DØ Inter-Cryostat Detector.

A variety of tests have shown that the LED Pulser System has a gain resolution of 0.2% and is stable over both short and long time scales.

Using this knowledge, the LED Pulser System may also be used as a calibration system to correct for gain changes in a PMT. If a detector is calibrated at initial time t_0, and using the LED Pulser System has PMT amplitude $\mathcal{A}_{PMT}(t_0)$ and PIN amplitude $\mathcal{A}_{PIN}(t_0)$, then the corrected amplitude, $\mathcal{A}^{cor}_{PMT}(t)$, using the calibration factor $\mathcal{F}_{\mathcal{A}}(t)$ is:

$$\mathcal{A}^{cor}_{PMT}(t) = \mathcal{F}_{\mathcal{A}} \times \mathcal{A}_{PMT}(t) = \frac{\mathcal{A}_{PMT}(t_0)}{\mathcal{A}_{PMT}(t)} \times \frac{\mathcal{A}_{PIN}(t)}{\mathcal{A}_{PIN}(t_0)} \times \mathcal{A}_{PMT}(t) \tag{8}$$

References

[1] L. Bartoszek, et al., (The E760 Collaboration), *The E760 Lead Glass Central Calorimeter: Design and Initial Test Results*, Nuclear Instruments and Methods in Physics Research A301 (1991) 47-60.

[2] S. Abachi, et al., (The D0 Collaboration), *The D0 Upgrade: Forward Preshower, Muon System, and Level 2 Trigger*, FERMILAB-FN-641, April 1996.

[3] B.S. Acharya et al., *Scintillation Counters for the DØ Muon Upgrade*, Nuclear Instruments and Methods A401 (1997) 45-62.

[4] V. Abramov, et. al., *Fast Scintillation Counters for the D0 Muon System Upgrade*, IEEE Transactions on Nuclear Science 46 (1999) 865-868.

[5] B. Baldin et al., *D0 Upgrade Muon Electronics Design*, IEEE Transactions on Nuclear Science 42 (1995) 736-742.

[6] B. Baldin, et al., "*D0 Muon Readout Electronics Design*, IEEE Transactions on Nuclear Science 44 (1997) 363-369.

[7] Bicron Corporation, 12345 Kinsman Road, Newbury, OH 44065.

[8] Nichia America Corporation, 3775 Hempland Road, Mountville, PA 17554.

[9] E.C. Dukes, *Monte Carlo Results on the Design of Light Guides for Scintillation Fiber Calorimeters*, Proceedings of the First International Conference on Calorimetry in High Energy Physics (1990) 177-188. DØNote 3299.

[10] Hewlett–Packard Company, 3000 Hanover Street, Palo Alto, CA 94304-1185.

[11] Hamamatsu Corporation, 360) Foothill Road, Bridgewater, NJ 08807.

[12] Anton, G., K. Büchler, and M. Kückes, *An LED Monitoring System for Pulse Height and Time Measurement with Scintillation Counters*, Nuclear Instruments and Methods in Physics Research A274 (1989) 222-226, North Holland, Amsterdam.

[13] Wire Pro Incorporated, 90 West Broadway, Salem, NJ 08079.

[14] Molex Incorporated, 2222 Wellington Court, Lisle, IL 60532-1682.

[15] Phillips Electronics North America, 1251 Avenue of the Americas, New York, NY 10020.

[16] Hanlet, P., et al., *Comparison of Fiber Polishing Techniques*, DØ Note 3561.

[17] D. Green, et al., *Accurate 2 Dimensional Drift Tube Readout Using Time Division and Vernier Pads*, Nuclear Instruments and Methods in Physics Research A256 (1987) 305-312.

[18] Doulas, S., et al., *DØ Muon Scintillator Phototube Gain Determination*, DØ Note 3861.